

## THE CONNECTION BETWEEN CONVECTIVE DOWNFLOWS AND SPINES IN A SUNSPOT PENUMBRA

G.B. SCHARMER<sup>1,2</sup> J. DE LA CRUZ RODRIGUEZ<sup>3</sup> P. SÜTTERLIN<sup>1,2</sup> V.M.J. HENRIQUES<sup>1,2</sup>

<sup>1</sup>Institute for Solar Physics, Royal Swedish Academy of Sciences, AlbaNova University Center, SE 106 91 Stockholm, Sweden  
<sup>2</sup>Stockholm Observatory, Dept. of Astronomy, Stockholm University, AlbaNova University Center, SE 106 91 Stockholm, Sweden

<sup>3</sup>Department of Physics and Astronomy, Uppsala University, Box 516, SE 751 20 Uppsala, Sweden

*Draft version March 30, 2019*

### ABSTRACT

We discuss NICOLE inversions of Fe I 630.15 nm and 630.25 nm Stokes spectra from a sunspot penumbra, recorded with the CRISP imaging spectropolarimeter at the Swedish 1-m Solar Telescope and a spatial resolution close to  $0''.15$ . Our emphasis is on narrow downflow lanes, which are cospatial with the relatively dark and cool parts of penumbral filaments. We find that these downflow lanes are located at the boundaries between areas of relatively horizontal magnetic field (the inter-spines) and much more vertical field (the spines). These locations agree with predictions from the convective gap model (the “gappy penumbra”) proposed six years ago, and more recent 3D MHD simulations. We also find that in the deep photosphere, the downflow lanes are frequently, but not always, associated with opposite polarity magnetic field. This is also consistent with the simulations, predicting that many of the convective downflows pull down the magnetic field, rather than flow passively along it.

*Subject headings:* Sunspots — Convection — Sun: magnetic topology — Sun: photosphere — Sun: surface magnetism

### 1. INTRODUCTION

The strong, nearly horizontal and radial outflows discovered more than 100 years ago (Evershed 1909), have inspired 1-dimensional (1D) numerical modeling of the penumbral filaments as flux tubes, with a siphon flow indirectly driven by the assumed difference in magnetic field strength between the ascending (in the penumbra) and descending (outside the penumbra) parts of magnetic flux tubes (Meyer & Schmidt 1968; Montesinos & Thomas 1989, 1997). Schlichenmaier et al. (1998b,a) instead modelled these flows as transient flows triggered by heating of thin flux tubes embedded in a convectively unstable penumbral atmosphere of given properties. However, neither of these models can provide the overall heat flux needed to explain the radiative losses of the penumbra (Schlichenmaier & Solanki 2003; Spruit & Scharmer 2006). For this, efficient convection is needed, with *vertical* RMS velocities comparable to those of the quiet Sun.

Spruit & Scharmer (2006) proposed that the penumbral filamentary structure and complex magnetic field topology is the result of convection opening up radially aligned, essentially field-free gaps. Sánchez Almeida (2005) and Sánchez Almeida & Ichimoto (2009) proposed to explain observed penumbral Stokes profiles in terms of spatially *unresolved* fluctuations in velocity and magnetic field, the Micro-Structured Magnetic Atmospheres (MISMAs). Recent simulations (Heinemann et al. 2007; Rempel et al. 2009; Rempel 2011, 2012) clearly support the presence of strong penumbral convection at *observable* scales, and lead to the surprising conclusion that the Evershed flow is identical to the horizontal component of this convection (Scharmer et al. 2008a; Rempel et al. 2009). This interpretation of penumbral fine structure is however not without controversy, the main argument being that observational evidence for convective *downflows* well inside the outer boundary of the penumbra is missing (Franz & Schlichenmaier 2009). Recently, such evidence was reported in the C I 538.03 nm

line (Scharmer et al. 2011; Joshi et al. 2011) and the Fe I 630.15 nm line (Scharmer & Henriques 2012), based on observations with the Swedish 1-m Solar Telescope (SST; Scharmer et al. 2003) and its imaging spectropolarimeter CRISP (Scharmer 2006; Scharmer et al. 2008b). Synthetic spectra calculated from simulations (Rempel 2011) confirm that such downflows should be visible in the C I 538.03 nm line at the spatial resolution of the SST (Bharti et al. 2011). In the present paper, we apply Stokes inversions to Fe I 630.15 nm and 630.25 nm spectra to establish the morphological connection between the convective downflows and the magnetic field in a sunspot penumbra.

### 2. OBSERVATIONS AND DATA REDUCTION

The observed data analyzed in this Letter are of a reasonably symmetric sunspot at approximately  $15^\circ$  heliocentric distance, obtained on 23 May 2010 with the SST and its imaging spectropolarimeter CRISP. These data are identical to those described recently (Scharmer et al. 2011; Scharmer & Henriques 2012), but here we include the 630.2 nm line in the analysis and a continuum wavelength 60 pm redward of the 630.2 nm line, adding to the 15 wavelengths scanned for each of the Fe I 630.15 and 630.25 nm lines. A complete scan of the two Fe I lines required only 16.5 s observing time.

We first compensated the images for darks and the “raw” flats similar to as described by Schnerr et al. (2011), and then processed the images with the MOMFBD code of van Noort et al. (2005). This was followed by a small-scale dewarping of the images to remove remaining alignment errors from high-altitude seeing at arc second scale, which cannot be compensated for by the  $4'' \times 4''$  subfield MOMFBD processing (Henriques 2012). We derived the transmission profile of CRISP and the pre-filter at each pixel, as well as a “true” flat-field image at each wavelength, by comparing the observed flat-field spectra, obtained close to disk center, to the FTS atlas spectrum (Brault & Neckel 1987; see Neckel 1999). The method used goes beyond that described

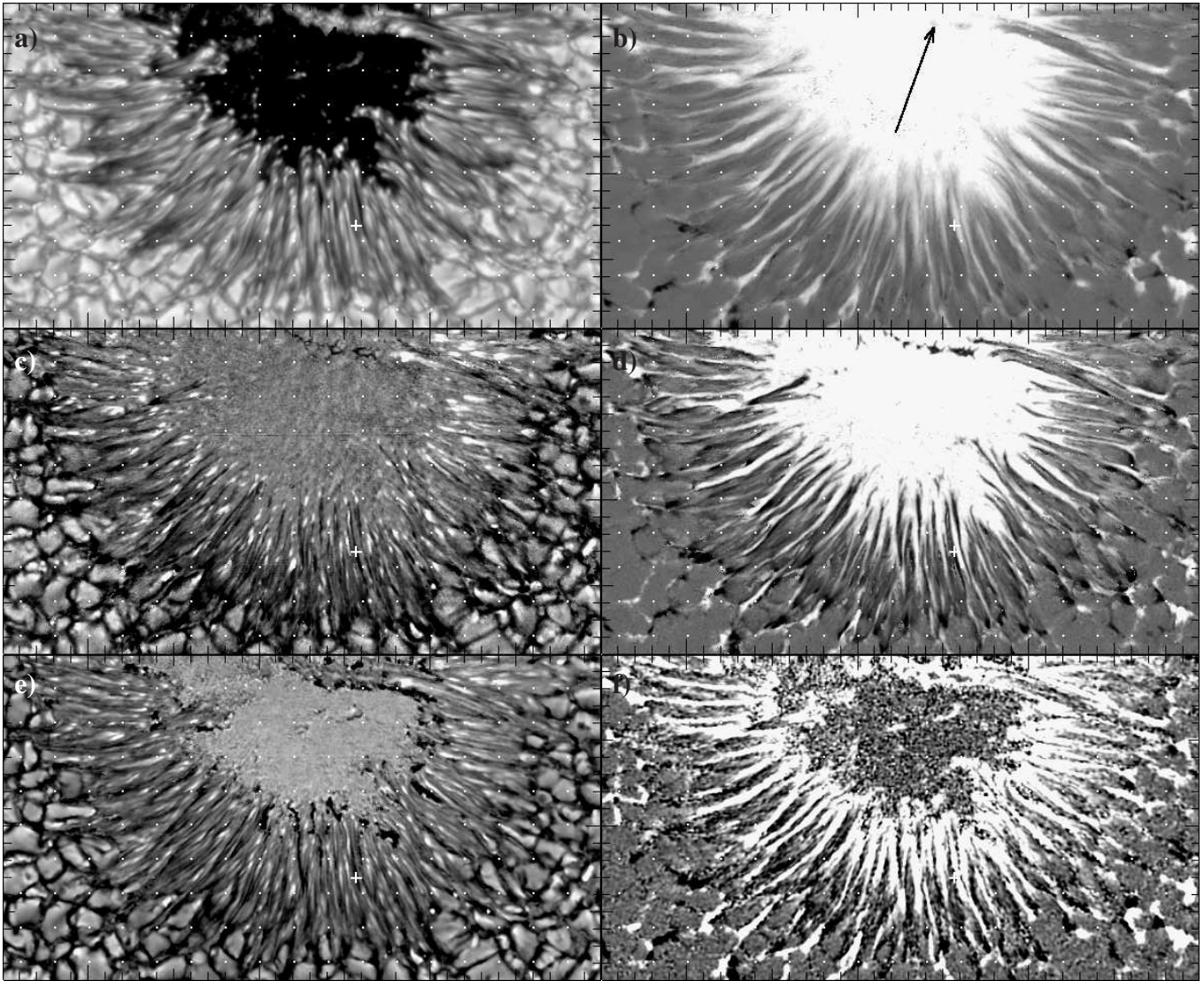


**Figure 1.** The left column (top to bottom) shows the temperature (scaled from 5000 K to 6600 K) at  $\tau_c = 1$ , the LOS velocity obtained at  $\tau_c = 1$  from inversions applied to the Fe I 630.15 nm and 630.25 nm lines, and the line core velocity of the C I 538.03 nm line. The right column shows (top to bottom) the LOS magnetic field (saturated at -1000 G and 1400 G) obtained at  $\tau_c = 0.02$  and  $\tau_c = 1$  from inversions of the Fe I lines, and the signed integrated circular polarization of the C I 538.03 nm line. Tick marks are at  $1''$  intervals, white dots are separated by  $2''$ . The arrow points in the direction of disk center. The FOV is  $\sim 35 \times 19''$ .

in Scharmer et al. (2008b) by using analytical expressions for the transmission profiles of the two etalons (c.f., Scharmer 2006), including the first side lobe on each side of the main peak for the high-resolution (HR) etalon. The free parameters of the fit are the wavelength shifts of the two etalons, the reflectivity of the HR etalon and the parameters of an assumed quadratic variation of the pre-filter transmission with wavelength. Including the side lobes of the HR etalon transmission profile returned excellent fits and an average reflectivity (93.44%) that is very close to that given by the manufacturer of the etalon coating (93.56%), suggesting very low levels of spectral straylight. From the fits, we also determine and compensate for the telluric blend in the red wing of the 630.25 nm line. In particular, this allows the inversions to take into account any asymmetries in the transmission profile resulting from the *relative* wavelength shifts of the peak transmissions of the two Fabry-Perot etalons. Such asymmetries could otherwise lead to errors in the LOS velocity gradient.

We also re-determined the polarization properties of the SST, using calibration data obtained with a 1-m rotating linear polarizer mounted in front of the SST in May, June and

October 2011. After demodulation of the MOMFBD restored images with an improved version of the polarization model of Selbing (2005), we checked the data for residual cross-talks from  $I$  to  $Q$ ,  $U$  and  $V$  and from  $V$  to  $Q$  and  $U$  using methods similar to those described by Schlichenmaier & Collados (2002). The cross-talks found were 0.3% or less from  $I$  to  $Q$ ,  $U$  and  $V$ , 2.7% from  $V$  to  $U$ , and much smaller from  $V$  to  $Q$ . These cross-talks were compensated for.

As the final step of our pre-processing, we compensated the data for stray-light (Scharmer et al. 2011; Scharmer & Henriques 2012). We assume the following relation between the observed  $I_o$  and “true”  $I_t$  intensities at any wavelength and polarization state:  $I_o = (1 - \alpha)I_t + \alpha I_t * G(W)$ , where  $\alpha$  is the straylight fraction, “ $*$ ” denotes convolution, and  $G$  is a Gaussian straylight point-spread function (PSF), having a full width at half maximum of  $W$ . For the present inversions, we set  $W$  to  $1''.8$  and  $\alpha$  to 0.4, rather than to  $1''.2$  and 0.5 respectively, as used previously (Scharmer & Henriques 2012). Our present choice of straylight parameters give similar RMS contrast for granulation, and similar up- and down-flow velocities in the penumbra, but result in fewer failures

with the inversion code. The wavelength scale (used for establishing the LOS velocity reference) was set by comparing the observed line profiles for granulation surrounding the sunspot, and void of strong fields, with those of 3D simulations (de la Cruz Rodríguez et al. 2011).

### 3. INVERSIONS

Inversions were applied jointly to the two Fe I lines. Abundances and atomic parameters used are identical to those of Socas-Navarro (2011). Inversions were made assuming a single atmospheric component in each pixel, excluding straylight compensation beyond that of the pre-processing (Sect. 2). We used the inversion code NICOLE, which is an improved implementation of the inversion code of Socas-Navarro et al. (2000). NICOLE was modified to accept a separate transmission profile for each pixel and was applied iteratively to the data with an increasing number of free parameters (FP), similar to as described by Socas-Navarro (2011). We used the following final number of FP: 3 each for temperature and the LOS velocity, 2 each for  $B_x$ ,  $B_y$  and  $B_z$ , and 1 for the micro-turbulence (13 FP). We used linear/quadratic interpolation in  $\log \tau_c$  of the corresponding atmospheric variables with 2/3 FP. We also made inversions with 3 FP for  $B_z$  in order to check that the inferred polarity reversals (Sect. 5) at continuum optical depth  $\tau_c=1$ , are robust results, which is the case. Indeed, we find that the opposite polarity patches seen with 2 FP for  $B_z$  are stronger and/or spatially more extended when using 3 FP. We also see a few more opposite polarity patches in the inner penumbra with 3 than with 2 FP. However, the inversions with 3 FP for  $B_z$  show enhanced levels of random noise and we discuss here only the results obtained with 2 FP for  $B_z$ . We note that the final number of FP used in our inversions is smaller than used by Socas-Navarro (2011). This is a direct consequence of the spectral resolution of CRISP (about 6 pm at 630 nm) being smaller than for his SOT/Hinode data, reducing the “height” resolution along the LOS for our data. We made a total of 41 inversion experiments in order to explore the effects of changes in the pre-processing of the data and the number of FP, and spent considerable time verifying the robustness of our results.

Figure 1 shows the LOS component of the magnetic field in the observers frame. Using the angle between solar North and disk center and the heliocentric distance of the spot, we transformed the magnetic field to the local frame. We resolved the 180 degree ambiguity by defining an approximate center for the sunspot and choosing the azimuth angle offset (0 or 180 deg) for which the horizontal field at  $\tau_c=0.1$  is directed more outward than inward from the spot center (this procedure for resolving the 180 degree ambiguity is of course inappropriate outside the sunspot). Figure 2 shows the magnitude and orientation of the horizontal field for every tenth pixel, and the vertical field (color coded) in the local frame. As is evident, the horizontal field is approximately parallel to the penumbral filaments and there are no indications of major systematic errors from the above described procedure, or from the calibration of and compensation for the telescope polarization.

### 4. GENERAL APPEARANCE OF THE INVERSION RESULTS

As far as we know, Bellot Rubio et al. (2006) made the first measurements of LOS velocity (and temperature) *gradients* in a sunspot penumbra using inversion techniques applied to data from an *imaging* spectrometer. Here, we estimate gradients of both the magnetic field and the LOS velocity from CRISP data for the first time, and the question arises whether

the results are meaningful and credible. We have investigated the velocity and magnetic maps returned by NICOLE over the entire  $55'' \times 55''$  FOV and note the following:

- 1) Isolated magnetic bright points and the interiors of larger flux concentrations (plage and pores) show a LOS magnetic field that decreases in strength with height, whereas at the boundaries of plage field the LOS magnetic field *increases* in strength with height. These results are consistent with observations, models and simulations of flux tubes expanding with height (e.g., Solanki et al. 1999; Yelles Chaouche et al. 2009; Pietarila et al. 2010, and references therein).
- 2) In the umbra, the light bridge and several bright umbral dots show a LOS magnetic field increasing in strength with height (as earlier described by Riethmüller et al. 2008), consistent with a field that wraps around and closes above structures that have weak field, or are nearly field-free, deeper down (c.f., Figs. 1b and 1d for examples).
- 3) In the penumbra, the interiors of magnetic spines (Lites et al. 1993) show a LOS magnetic field that decreases in strength with height (as is evident by comparing Figs. 1b and 1d), but at the *boundaries* of the spines, the LOS magnetic field strength *increases* with height, consistent with canopy fields folding over the inter-spines (the “gaps”). Similar magnetic field topologies were first described by Borrero et al. (2008).
- 4) Examination of the map of the transverse field (Fig. 2) shows a clear tendency for the transverse field to diverge away from the penumbral spines, qualitatively consistent with flux conservation and the strong decrease of the strength of the LOS field with height in the spines.
- 5) For the brightest umbral dots, the transverse field is much stronger on the *disk center* side than on the limb side in the deep layers, consistent with a field that folds over these dots.
- 6) The measured LOS velocities decrease in strength with height almost everywhere in the FOV, in qualitative agreement with e.g Franz & Schlichenmaier (2009), and as expected for overshooting convection.

We will discuss some of these aspects of our Fe I data in forthcoming publications.

Figure 1 shows the  $35'' \times 19''$  sub-field discussed in this Letter. This Figure illustrates that the Fe I LOS *velocity field* at  $\tau_c = 1$  (Fig. 1c) in the quiet Sun and penumbra is very similar to that of the C I line core (Fig. 1e), formed in the deep photosphere (Schlichenmaier & Schmidt 1999). We also note that the penumbral LOS magnetic field maps at  $\tau_c = 1$  (Fig. 1d) and the deeply formed C I line (Fig. 1f) show a number of nearly co-spatial opposite polarity patches, whereas in many cases no such opposite patches can be seen in the Fe I lines at  $\tau_c = 0.02$  (Fig. 1b). We thus find several independent pieces of evidence supporting our claim that the inversions return trustworthy information about the height variations of the LOS velocity and magnetic field.

### 5. DARK DOWNFLOW LANES

Figure 3a shows the temperature map at  $\tau_c = 1$ , with the narrow dark redshifted lanes seen at  $\tau_c = 1$  in Fig. 1c overlaid in red. Several such lanes are clearly visible where the radial direction of the filaments is close to  $\pm 90^\circ$  from the disk center direction (the uppermost parts of the panels). At these locations, there are no contributions from the radial Evershed flow, such that we conclude that *these narrow and long redshifted lanes represent downflow lanes*. Many similar looking narrow lanes, but with stronger redshifts, can be seen at the limb side penumbra, strongly suggesting that they are also downflow

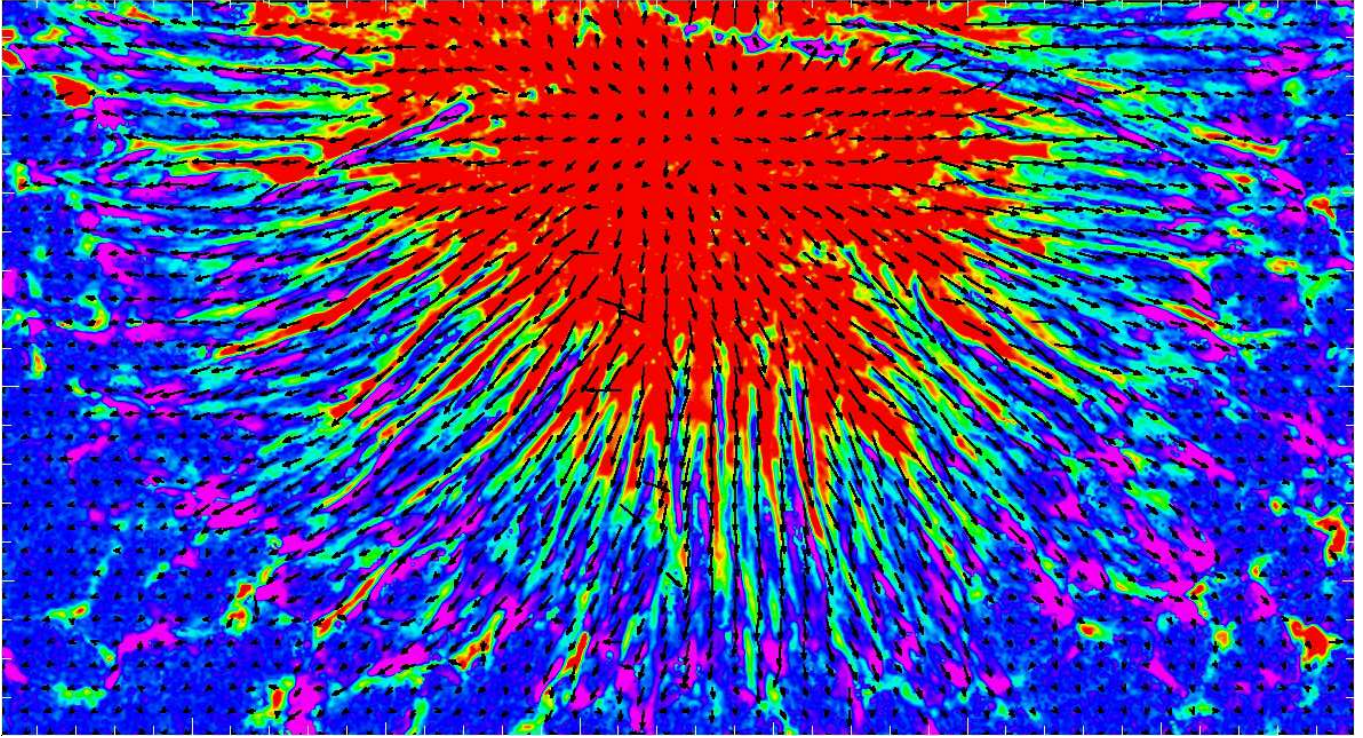


**Figure 2.** The Figure shows the orientation (direction of the arrows) and strength (proportional to the lengths of the arrows) of the horizontal magnetic field at an optical depth of  $\tau_c = 0.1$ , after transformation to the local frame. The vertical magnetic field (also in the local frame) is shown at  $\tau_c = 1$  and is encoded in color such that red corresponds to field of the same polarity as the spot and stronger than about 1500 G, and violet to opposite polarity field stronger than about 300 G. The arrows are plotted for every tenth pixel (corresponding to  $0''.59$ ), and give only a low-resolution view of the horizontal field. Tick marks are at  $1''$  intervals. The FOV is  $\sim 35 \times 19''$  and corresponds to that shown in Fig. 1.

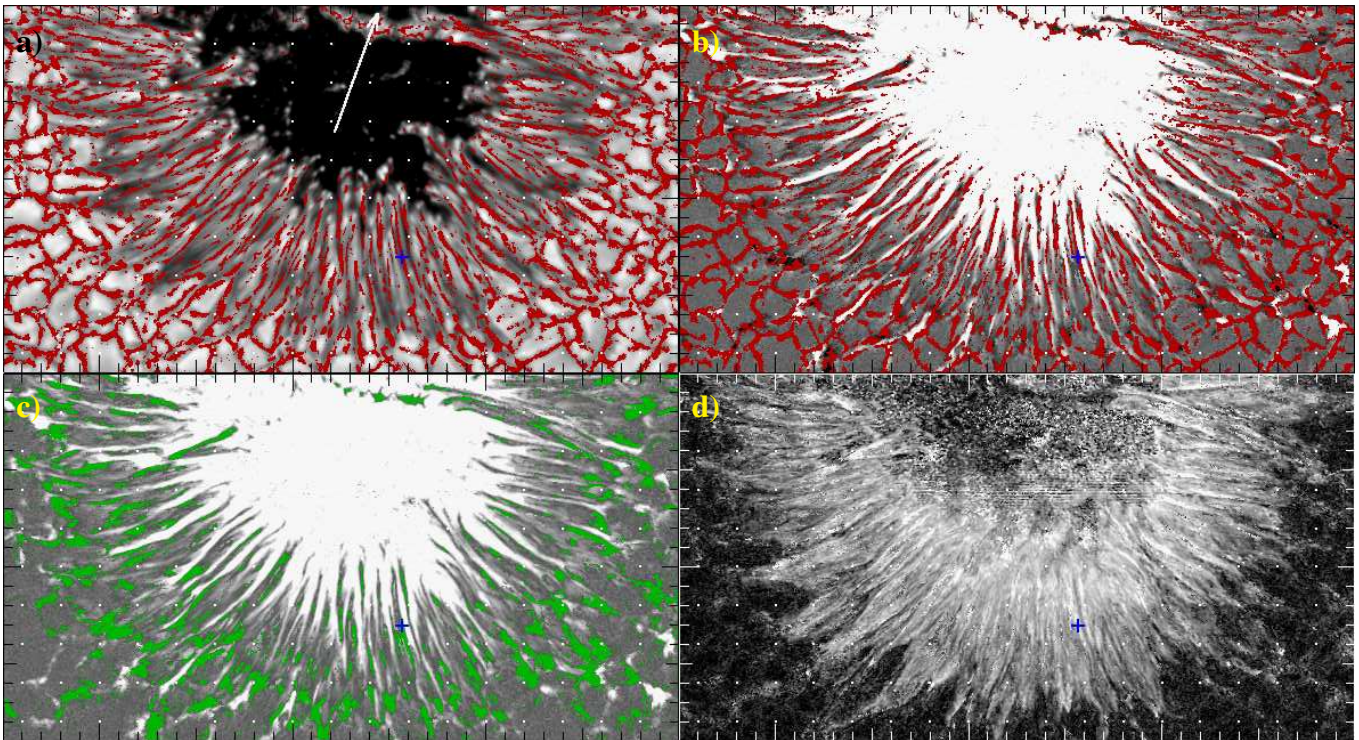


**Figure 3.** The top panel shows the temperature (scaled from 5000 K to 6600 K) at  $\tau_c = 1$ , with the dark downflow lanes at  $\tau_c = 1$  in Fig. 1, outlined in red. The second panel shows the same downflow lanes overlaid on a map of the vertical component (in the local frame) of the magnetic field (scaled as in Fig. 1) at  $\tau_c = 1$ . The third panel shows the vertical magnetic field, with opposite polarity field less than -200 G indicated in green. The fourth panel shows the magnitude of the horizontal field (in the local frame) at  $\tau_c = 1$ , scaled from 150 G to 1800 G.

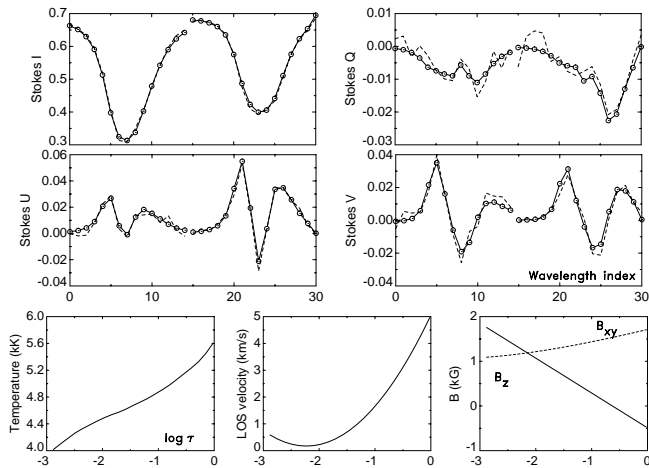


**Figure 4.** Observed (dashed) and fitted synthetic (solid) Stokes profiles in a downflow lane pixel, and the corresponding variations of temperature, LOS velocity, vertical (solid) and horizontal (dashed) magnetic field in the *local* frame. The 630.15/630.25 nm line profiles (plotted side by side) are normalized to the average continuum intensity outside the spot, and are shown for the pixel marked with “+” in Figs. 1 and 3.

lanes and that they are associated with strong outflows. This conclusion receives strong support by the *absence of narrow* blueshifted flow lanes on the disk center side. If the narrow lanes on the limb side instead were strong outflow lanes with (weak) *upflows*, they would show *stronger* Doppler signature (but with opposite sign) on the *disk center* side, where the LOS would be more or less aligned with the flow direction, than on the limb side. Since the opposite is true, we feel confident in our identification of these lanes as downflow lanes.

Figure 4 shows the observed and fitted synthetic Stokes profiles for a downflow lane pixel marked with “+” in Figs. 1 and 3. The Stokes V profiles are abnormal with 3 lobes instead of 2, but are nevertheless well fitted by the variations of the LOS velocity and *vertical* magnetic field (in the *local* frame) with  $\tau_c$ , shown in the lower panels. The polarity of the vertical magnetic field reverses below  $\tau_c = 0.2$ , and the magnitude of the horizontal field decreases rather strongly with height.

Comparing the temperature maps in Figs. 1a and 3a, it is clear that *almost all downflow lanes well inside the outer boundary of the penumbra are co-spatial with the relatively (compared to their immediate surroundings) cool parts of the penumbral filaments*, blinking the two maps makes this even more obvious (the opposite is not true: there are many relatively cool filamentary structures that are not associated with obvious downflow lanes). We conclude that these downflow lanes are part of the convective flows, and contribute to the intensity–vertical velocity correlation established in our previous work (Scharmer et al. 2011; Scharmer & Henriques 2012).

Figure 3b shows a remarkable relation between the location of the downflow lanes and the magnetic spines (shown white): well inside the penumbra, *most of the downflow lanes are located at the boundaries of the spines*, or, where the spines are very close together, between the spines.

Figure 3c shows in green color locations where the vertical magnetic field component (in the local frame) is of opposite polarity with a strength of more than 200 G. Most of this opposite polarity field is located close to the outer boundary of the penumbra and is associated with (in some cases very strong) downflows. In the interior parts of the penumbra, *many patches of opposite polarity field are co-spatial with the*

*narrow downflow lanes.*

The magnitude of the horizontal field at  $\tau_c=1$  shown in Fig. 3d demonstrates that the spine structure, which is obvious in the map of the vertical field, is *absent* in the horizontal field map. This means that the *horizontal* field is nearly as strong in the spines as in the inter-spines at this depth.

## 6. DISCUSSION

We have identified narrow downflow lanes in the interior penumbra that are co-spatial with the relatively cool parts of the penumbral filaments, and located at the *boundaries* of the magnetic spines. These locations agree with predictions of the convective gap model (Scharmer & Spruit 2006) and recent simulations (Rempel 2012, his Fig. 22). We also find that in most cases these downflow lanes are associated with opposite polarity field, supporting the identification of these lanes as downflow lanes. The absence of opposite polarity field associated with some downflow lanes also agrees with the simulations, showing that the downflows frequently pull down the magnetic field instead of just flowing passively along it.

The *horizontal* field inferred from our data is nearly as strong in the inter-spines as in the spines. This is consistent with the simulations of Rempel (2012), showing a layer of strong horizontal magnetic field near  $\tau_c = 1$ , and weak-field gaps located *below the visible surface*. The distinctly different morphologies of the penumbral horizontal and vertical field components shown in Fig. 3 are remarkably similar to those of the simulations (Rempel 2012, his Figs. 6b and 6c).

By calibrating the CRISP transmission profile at each pixel, we have been successful in using the inversion code NICOLE to simultaneously estimate LOS velocities, the magnetic field vector, and their LOS gradients from combined 630.15 nm and 630.25 nm Stokes spectra, at a spatial resolution close to  $0''.15$ . These results support earlier measurements in the deeply formed C I line. The present and earlier discussed (Scharmer et al. 2011; Scharmer & Henriques 2012) observational data, as well as simulations (Rempel 2012), and synthetic spectra obtained from simulations (Bharti et al. 2011), clearly illustrate the need for reaching this spatial resolution in order to resolve the convective downflows in the *interior* of sunspot penumbrae.

Dan Kiselman and Mats Löfdahl are thanked for comments on the manuscript. The Swedish 1-m Solar Telescope is operated on the island of La Palma by the Institute for Solar Physics of the Royal Swedish Academy of Sciences in the Spanish Observatorio del Roque de los Muchachos of the Instituto de Astrofísica de Canarias.

## REFERENCES

- Bellot Rubio, L. R., Schlichenmaier, R., & Tritschler, A. 2006, *A&A*, 453, 1117  
 Bharti, L., Schüssler, M., & Rempel, M. 2011, *ApJ*, 739, 35  
 Borrero, J. M., Lites, B. W., & Solanki, S. K. 2008, *A&A*, 481, L13  
 de la Cruz Rodríguez, J., Kiselman, D., & Carlsson, M. 2011, *A&A*, 528, A113+  
 Evershed, J. 1909, *MNRAS*, 69, 454  
 Franz, M., & Schlichenmaier, R. 2009, *A&A*, 508, 1453  
 Heinemann, T., Nordlund, Å., Scharmer, G. B., & Spruit, H. C. 2007, *ApJ*, 669, 1390  
 Henriques, V. M. J. 2012, *A&A*, in press  
 Joshi, J., Pietarila, A., Hirzberger, J., et al. 2011, *ApJ*, 734, L18+  
 Lites, B. W., Elmore, D. F., Seagraves, P., & Skumanich, A. P. 1993, *ApJ*, 418, 928

- Meyer, F., & Schmidt, H. U. 1968, *Mitteilungen der Astronomischen Gesellschaft Hamburg*, 25, 194
- Montesinos, B., & Thomas, J. H. 1989, *ApJ*, 337, 977
- . 1997, *Nature*, 390, 485
- Neckel, H. 1999, *Sol. Phys.*, 184, 421
- Pietarila, A., Cameron, R., & Solanki, S. K. 2010, *A&A*, 518, A50
- Rempel, M. 2011, *ApJ*, 729, 5
- . 2012, *ApJ*, 750, 62
- Rempel, M., Schüssler, M., Cameron, R. H., & Knölker, M. 2009, *Science*, 325, 171
- Riethmüller, T. L., Solanki, S. K., & Lagg, A. 2008, *ApJ*, 678, L157
- Sánchez Almeida, J. 2005, *ApJ*, 622, 1292
- Sánchez Almeida, J., & Ichimoto, K. 2009, *A&A*, 508, 963
- Scharmer, G. B. 2006, *A&A*, 447, 1111
- Scharmer, G. B., Bjelksjö, K., Korhonen, T. K., Lindberg, B., & Petterson, B. 2003, in *Society of Photo-Optical Instrumentation Engineers (SPIE) Conference Series*, Vol. 4853, *Society of Photo-Optical Instrumentation Engineers (SPIE) Conference Series*, ed. S. L. Keil & S. V. Avakyan, 341–350
- Scharmer, G. B., & Henriques, V. M. J. 2012, *A&A*, 540, A19
- Scharmer, G. B., Henriques, V. M. J., Kiselman, D., & de la Cruz Rodríguez, J. 2011, *Science*, 333, 316
- Scharmer, G. B., Nordlund, Å., & Heinemann, T. 2008a, *ApJ*, 677, L149
- Scharmer, G. B., & Spruit, H. C. 2006, *A&A*, 460, 605
- Scharmer, G. B., Narayan, G., Hillberg, T., et al. 2008b, *ApJ*, 689, L69
- Schlichenmaier, R., & Collados, M. 2002, *A&A*, 381, 668
- Schlichenmaier, R., Jahn, K., & Schmidt, H. U. 1998a, *ApJ*, 493, L121+
- . 1998b, *A&A*, 337, 897
- Schlichenmaier, R., & Schmidt, W. 1999, *A&A*, 349, L37
- Schlichenmaier, R., & Solanki, S. K. 2003, *A&A*, 411, 257
- Schnerr, R. S., de La Cruz Rodríguez, J., & van Noort, M. 2011, *A&A*, 534, A45
- Selbing, J. 2005, Master's thesis, Stockholm University
- Socas-Navarro, H. 2011, *A&A*, 529, A37
- Socas-Navarro, H., Trujillo Bueno, J., & Ruiz Cobo, B. 2000, *ApJ*, 530, 977
- Solanki, S. K., Finsterle, W., Rüedi, I., & Livingston, W. 1999, *A&A*, 347, L27
- Spruit, H. C., & Scharmer, G. B. 2006, *A&A*, 447, 343
- van Noort, M., Rouppe van der Voort, L., & Löfdahl, M. G. 2005, *Sol. Phys.*, 228, 191
- Yelles Chaouche, L., Solanki, S. K., & Schüssler, M. 2009, *A&A*, 504, 595